J Mol Model (2011) 17:2305–2311
DOI 10.1007/s00894-011-1059-7

ORIGINAL PAPER

Hydrogen sequential dissociative chemisorption on Ni_n(n = 2~9,13) clusters: comparison with Pt and Pd

Chenggang Zhou · Shujuan Yao · Qingfan Zhang · Jinping Wu · Ming Yang · Robert C. Forrey · Hansong Cheng

Received: 29 September 2010 / Accepted: 22 March 2011 / Published online: 27 April 2011

Abstract Hydrogen dissociative chemisorption and desorption on small lowest energy Ni_n clusters up to n=13 as a function of H coverage was studied using density functional theory. H adsorption on the clusters was found to be preferentially at edge sites followed by 3-fold hollow sites and on-top sites. The minimum energy path calculations suggest that H_2 dissociative chemisorption is both thermodynamically and kinetically favorable and the H atoms on the clusters are mobile. Calculations on the sequential H_2 dissociative chemisorption on the clusters indicate that the edge sites are populated first and subsequently several on-top sites and hollow sites are also occupied upon full cluster saturation. In all cases, the average hydrogen capacity on Ni_n clusters is similar to that of Pd_n clusters but considerably smaller than that of Pt_n clusters. Comparison of hydrogen dissociative chemisorption energies and H desorption energies at full H-coverage among the Ni family clusters was made.

C. Zhou · H. Cheng (✉)
Department of Chemistry, National University of Singapore,
Singapore 3 Science Drive 3,
Singapore 117543, Singapore
e-mail: chmch@cug.edu.sg

C. Zhou · Q. Zhang · J. Wu · M. Yang · H. Cheng
Sustainable Energy Laboratory,
China University of Geosciences (Wuhan),
Wuhan 430074, China

S. Yao
College of Materials Science and Engineering,
Liaocheng University,
Liaocheng 252059, China

R. C. Forrey
Department of Physics, Penn State University,
Berks Campus,
Reading, PA 19610–6009, USA

Keywords Hydrogen dissociative chemisorption · Nickel clusters · Palladium clusters · Platinum clusters

Introduction

Nickel family metals, including nickel, palladium and platinum, are three of the most important catalysts used in many industrial heterogeneous catalytic processes, such as steam reforming and hydrogenation/dehydrogenation reactions. These metal catalysts are usually prepared in a form of dispersed particles on various support materials. Numerous studies have demonstrated that nano-sized catalytic particles are more chemically active than bulk-sized catalyst of the same element [1]. As building blocks of bulk solids, small clusters of these metals often exhibit different physicochemical properties than those of bulk materials. Despite being in the same family in the periodic table, the properties of the metal elements differ considerably. Understanding of the relationships of these properties between this family of elements is of fundamental importance for design and development of novel catalysts, alloys and nanoparticles for specific applications. In the present study, we aim to address the common properties and differences of small clusters of the nickel family upon formation of hydrides under H_2-abundant environment using density functional theory (DFT). The hydrides of nickel and palladium have been used for applications in batteries [2], fuel cells [3] and hydrogen purifications [4, 5], and platinum has been shown to be an efficient catalyst for hydrogen dissociation [6].

Hydride formation of small Pd [7–9] and Pt [10, 11] clusters has been systematically addressed previously. It was found that interactions between hydrogen and these metals differ considerably [7–15]. The on-top sites were identified as energetically the most favorable binding sites

for H atoms on Pt clusters [10–14], while the hollow and edge sites are preferred on Pd clusters [7–9, 14, 15]. The capacity of Pt clusters to adsorb H atoms was found to be substantially higher than that of Pd clusters. Structures of small Ni clusters have also been studied extensively both experimentally [16–20] and theoretically [21–29]. It was found that Ni clusters are mostly magnetic and their magnetic moments diminish rapidly upon adsorption of hydrogen as the bonding changes gradually from metallic to covalent [20]. Ni clusters were capable of accommodating more hydrogen atoms than other transition metal clusters of the same size in the same row of the periodic table [30]. The cationic hydride complexes, $Ni_nH_m^+$, were studied by Swart et al. [31] using IR photon dissociation spectroscopy. For n=4, 5 and 6, they also calculated the hydride structures and vibrational spectra using DFT. It was found that upon saturation with atomic hydrogen via chemisorption, Ni clusters can continue binding with additional H_2 molecules via physisorption.

We have conducted a systematic study using DFT on hydride formation of small Ni_n (n=2–9, 13) clusters. In this paper, we report our computational results and compare the hydride formation properties of Ni clusters with those of Pd and Pt clusters with the goal of understanding the reactivity of these metal clusters with H_2. In particular, key properties of the metal clusters at full saturation by H atoms are systematically addressed. For catalytic reactions, these properties, which include H_2 dissociative chemisorption energy, H atom desorption energy, and the maximum capacity for accommodating H atoms, are particularly relevant since metal catalyst surfaces are in general fully covered by H atoms at a finite H_2 pressure. The comparative study would shed light on the catalytic performance of small clusters of the Ni family elements.

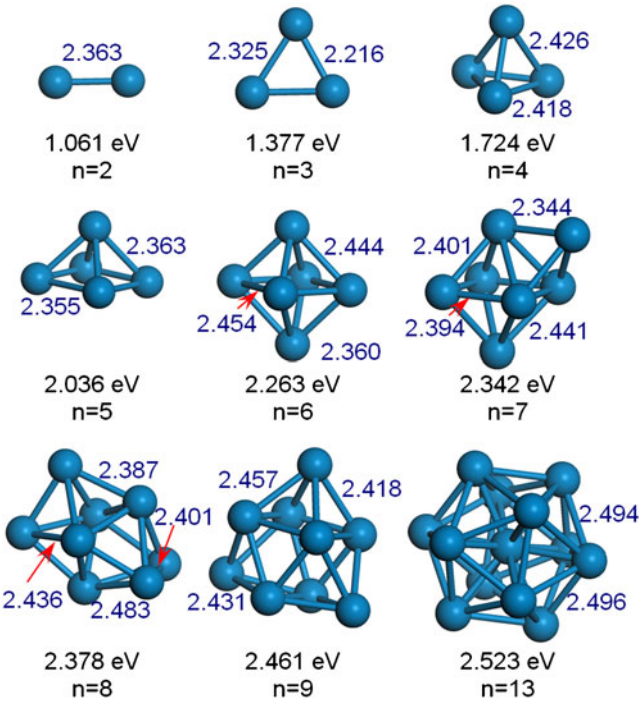

Fig. 1 The optimzied minimum energy structures of Ni_n (n=2–9, 13) clusters

Computational details

All calculations were performed using DFT/GGA (generalized gradient approximations) with the Perdew and Wang [32, 33] (PW91) exchange-correlation functional as implemented in the DMol^3 package [34, 35]. A double numerical basis set augmented with polarization functions was used to describe the valence electrons, while the core electrons were described by an effective core pseudopotential [36, 37]. These basis functions are numerically exact atomic orbitals rather than analytical functions (e.g., Gaussian or Slater type orbitals) and molecules can be dissociated exactly to its constituent atoms within the DFT context. It has been shown that this quality of basis set gives rise to very little superposition effects [38]. A spin-polarized scheme was employed to deal with the electronically open-shell systems intrinsic to the Ni atoms. Charge transfer was calculated using the Hirshfeld population scheme [39]. The method employed in the present study has been successfully utilized to study bulk properties of the transition metal elements and good agreement between the calculated structures and cohesive energies and the available experimental values were achieved [13–15]. To facilitate SCF convergence, small charge smearing was initially applied to the low lying virtual states and subsequently the smearing value was completely removed upon the SCF convergence with a tolerance of 1.0×10^{-6} Ha.

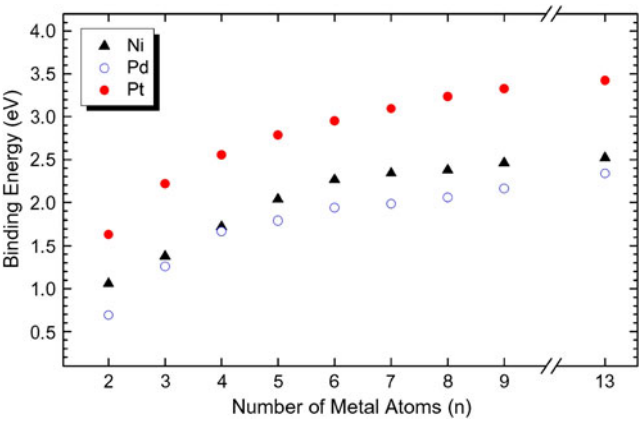

Fig. 2 Comparison of the calculated binding energies of small Ni, Pd and Pt clusters

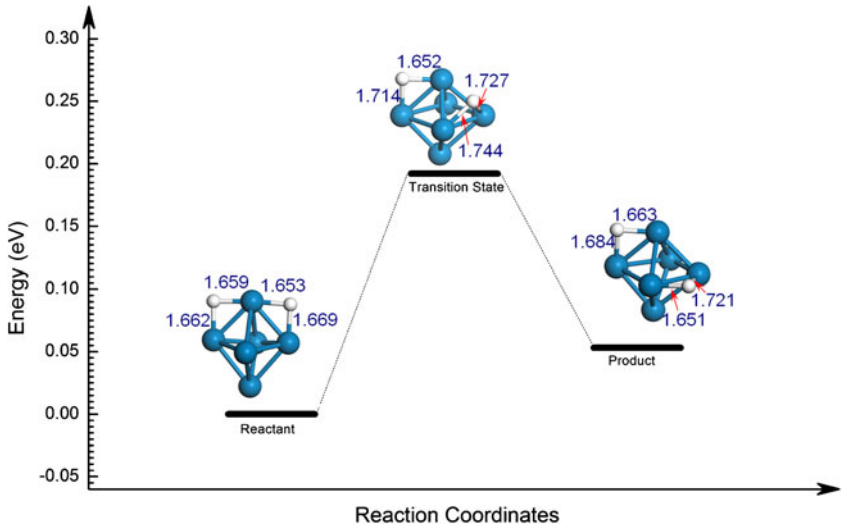

Fig. 3 The calculated energy diagram of H migration pathway

All structures were fully optimized without symmetry constraints. The energetically most stable structures were found using the conjugated gradient algorithm. The transition state (TS) structure search using the LST/QST algorithm [40] was conducted only for H_2 on Ni_6 to gain insight into the H_2 dissociative chemisorption kinetics and for H atom diffusion in the cluster. The optimization tolerance was set to be 1.0×10^{-5} Ha. The obtained TS structure was further verified by normal mode analysis that yields only one imaginary frequency. For the clusters with a given size, an exhaustive search for minimum energy structures was conducted. The average binding energy (ΔE_{BE}) of a cluster containing *n* Ni atoms can be calculated using:

$$\Delta E_{BE} = (nE_{Ni} - E_{Ni_n})/n,\ (n = 2,\ 3,\ \ldots) \tag{1}$$

where E_{Ni} and E_{Ni_n} represent the energies of a single Ni atom and the Ni_n cluster, respectively. The average dissociative chemisorption energy per H_2 and sequential desorption energy per H atom were evaluated using the following equations:

$$\Delta E_{CE} = 2(E_{Ni_n} - E_{Ni_nH_m})/m + E_{H_2},\ (n = 2,\ 3\ldots;\ m = 2,\ 4,\ 6,\ \ldots) \tag{2}$$

$$\Delta E_{DE} = E_H - (E_{Ni_nH_m} - E_{Ni_nH_{m-2}})/2,\ (n = 2,\ 3\ldots;\ m = 2,\ 4,\ 6,\ \ldots). \tag{3}$$

At full H saturation, the sequential desorption energy ΔE_{DE} represents the threshold energy required for an H atom to desorb from the cluster surface. To identify the full H saturation state of the Ni clusters, we performed room temperature *ab initio* molecular dynamics (AIMD) simulations for 3 ps in a NVT canonical ensemble using the Nosé-Hoover thermostat [41]. Excessive H atoms on the cluster will recombine to form H_2 molecules upon the AIMD simulation.

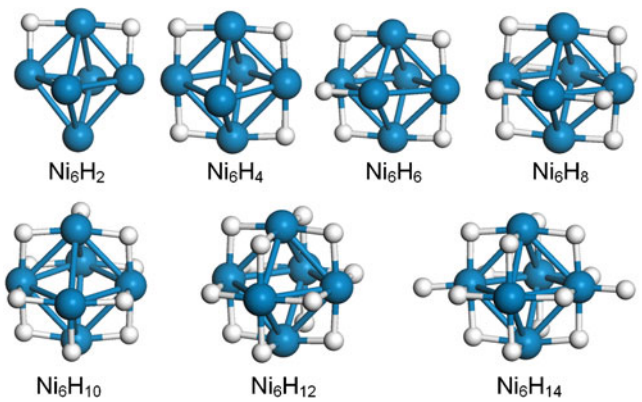

Fig. 4 Sequential loading of H atoms on the Ni_6 cluster until full H saturation

Results and discussion

Similar to small Pd and Pt clusters, numerous isomers exist for Nickel clusters with a given size. We first performed geometry optimizations to identify the stable structures of small Ni clusters. Figure 1 depicts the lowest energy structures and the average binding energies for Ni_n (n=2~9, 13). Our results are consistent with the reported theoretical studies on small Ni clusters [42, 43]. As expected, the calculated lowest energy cluster of a given size exhibits similar structural characteristics to the same size of Pt and Pd cluster and the Ni clusters undergo a similar triangular growth pathway. The calculated average binding energies of Ni_n clusters, together with the values of Pt and Pd calculated previously [44, 45], are shown in

Fig. 2. As expected, the average binding energy increases with the cluster size monotonically. For the same cluster size, the binding strength of the Ni cluster is similar to that of the Pd cluster but smaller than that of the Pt cluster. Interestingly, the relative binding strength of small clusters shown in Fig. 2 is consistent with the trend of the cohesive energies of the bulk Ni, Pd and Pt solids reported experimentally (Ni: 4.44 eV; Pd: 3.89 eV; Pt: 5.84 eV [46]).

We next studied the sequential H_2 dissociative chemisorption on the lowest energy Ni clusters. For n=2, hydrogen prefers to reside on the edge. For n≥3, three possible adsorption sites, i.e., one-fold on-top, two-fold edge and three-fold hollow, are available to accommodate hydrogen atoms. Regardless of the cluster size, we found that the most favorable site for hydrogen on Ni_n clusters is on the edge, followed by the hollow site and the on-top site is the least stable. The bonding preference for hydrogen on the Ni clusters is distinctively different from the case of Pt and Pd clusters. For small Pd clusters [14, 15], the sequence of H binding preference is the hollow site followed by the edge site and non-bonding at the on-top site, while for small Pt clusters [12, 13], the on-top site is the strongest binding site, followed by the edge site and then the hollow site. The relative binding preference for H atoms correlates well with the average binding energy of the metal clusters. H atoms prefer to be absorbed on-top on relatively strong binding clusters, such as Pt_n, and fall into the hollow sites on relatively weaker binding clusters like Pd_n to maximize the interaction with more metal atoms.

To simplify the presentation, we chose the Ni_6 cluster as an example for detailed analysis of sequential H_2 dissociative chemisorption and H diffusion. We sampled several initial configurations for a H_2 molecule to approach the cluster. It was identified that the pathway starting from a

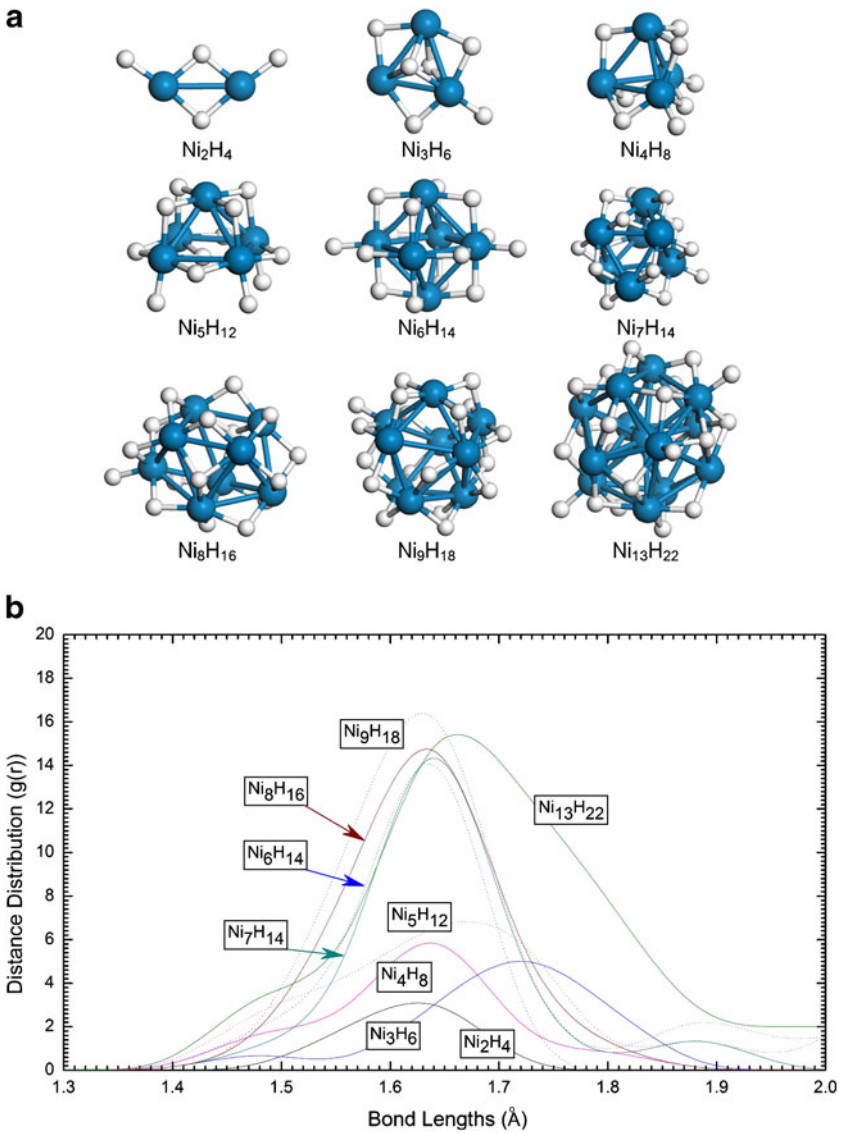

Fig. 5 (**a**) The fully saturated hydrides of the selected Ni_n (n=2–9, 13) clusters and (**b**) The calculated Ni-H bond distance distribution of the nickel hydrides

side-on configuration of H_2 to interact with an on-top Ni atom that leads to H adsorption on two neighboring edge sites to be energetically most favorable. The dissociation process is essentially barrierless, similar to the situation of H_2 dissociation on Pd and Pt clusters. The calculated adsorption energy is 1.31 eV, slightly higher than the value on Pd_6 (1.16 eV) but considerably lower than on Pt_6 (1.61 eV). We next studied the mobility of the absorbed H atoms on the cluster by moving a H atom from the edge site to a nearby edge. Figure 3 displays the calculated energy diagram of the migration pathway, where the optimized initial, transition state and final structures are also shown. The H migration requires 0.19 eV activation energy and is essentially thermal neutral. The H migration barrier on Ni_6 is slightly higher than on Pd_6 (0.11 eV) and slightly lower than on Pt_6 (0.23 eV). The modest difference in the calculated H migration barriers among these clusters correlates well with the relative stability of hydrogen on the clusters. In general, the results suggest that H migration on the Ni family clusters is facile.

Next, we considered sequential loading of H_2 molecules on the cluster until full saturation. The fully optimized structures of sequentially dissociated H_2 molecules on the cluster are shown in Fig. 4. Again, the edge sites of the cluster are populated first at low coverage. As the H loading increases, the edge sites become fully occupied and two on-top sites opposite to each other are also populated. The Ni_6 cluster reaches full saturation at m=14, beyond which excessive H atoms will recombine to form H_2 molecules. The maximum hydrogen capacity of Ni_6 is the same as that of Pd_6, despite the fact that the size of Pd_6 is considerably larger than Ni_6. We note that Ni_6 has 12 edge sites, which are fully occupied by H atoms, with two opposite on-top sites available to accommodate additional two H atoms. On Pd_6, however, there are only 8 three-fold hollow sites available for H atoms with additional six edges for H atom access. Not surprisingly, the hydrogen capacities of Ni_6 and Pd_6 are both significantly lower than that of Pt_6 which not only has higher binding strengths with H atoms but also allows H atoms to reside at the on-top sites.

Similar to Ni_6, our calculations on H_2 dissociative chemisorption on other Ni_n clusters at low H coverage suggest that the process is both kinetically and thermodynamically favorable and the H atoms on the cluster are mobile. Figure 5a displays the structures of small Ni_n clusters at full H saturation. These structures were obtained upon full AIMD runs at room temperature to ensure that all H atoms are chemisorbed and hollow sites are also occupied by H atoms. The simulated Ni-H distance distributions of these hydrides are shown in Fig. 5b. Most of the Ni-H bonds are between 1.6–1.7 Å, slightly shorter than the Pd-H bonds (1.7–1.8 Å [12–14]) in Pd hydrides and considerably shorter than the Pt-H bonds (2.2–2.3 Å [14, 15]) in Pt hydrides.

Figure 6a compares the calculated average H_2 dissociative chemisorption energies (ΔE^T_{CE}) of Ni_n, Pd_n and Pt_n clusters at full saturation. Remarkably, they all vary in a small energy range between 0.6 eV and 1.0 eV regardless of the cluster size except for Pd_2 and Pd_3, which exhibit considerably higher average H_2 dissociative chemisorption energies. The results imply that clusters of the three metal elements behave similarly in terms of dissociating H_2 molecules at full H coverage. The size-independence is largely due to the fact that the chemical bonding of the clusters evolves from metallic to covalent as H atoms are sequentially loaded up onto the clusters. As a consequence, the chemical properties become localized and thus do not depend strongly on cluster size. We note that at typical catalytic hydrogenation conditions the metal catalysts are fully covered by H atoms. For a given catalyst quantity, smaller catalyst particles offer higher surface area exposed to the gas species. However, our results suggest that H_2 dissociative chemisorption energies do not change significantly with particle size. This makes computational modeling of surface catalysis convenient because one could select a relatively small size cluster to represent catalyst particles. Similarly, we calculated H atom desorption energies (ΔE^T_{DE}) at full H coverage of the metal clusters and the results are displayed in Fig. 6b. The desorption energy at full H coverage is an important physical quantity

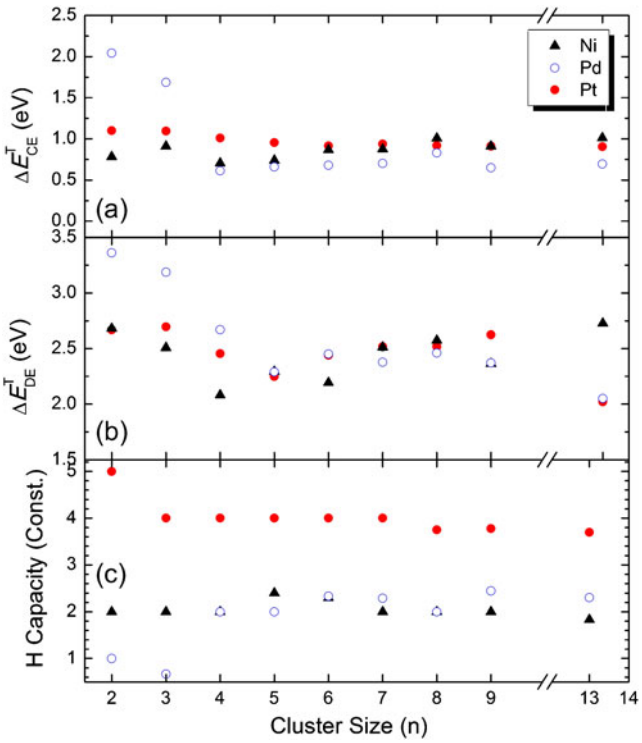

Fig. 6 Comparison on (**a**) the threshold of H_2 dissociative chemisorptions energy, (**b**) the threshold of H desorption energy and (**c**) maximum H capacity of small Ni, Pd and Pt clusters

because it can serve as an indicator of catalytic activity. A small desorption energy indicates higher activity. For small Ni_n clusters, the H desorption energy varies in a range between 2.08 to 2.73 eV. The highest desorption energy is observed for Ni_{13}, sharply higher than the values of Pd_{13} and Pt_{13}. The results suggest that it is more difficult to pull H atoms out of the Ni catalyst than out of Pd and Pt catalysts. Figure 6c displays the calculated average H capacities of Ni_n, Pd_n and Pt_n clusters per atom. Essentially, each Pt atom is capable of adsorbing 4 H atoms, while each Ni or Pd atom can only accommodate 2 H atoms.

Summary

We used DFT to investigate hydride formation on small Ni_n clusters. We compared key chemical properties of the clusters with those of Pd_n and Pt_n clusters. It was found that small Ni_n clusters grow in a similar pathway to Pd_n and Pt_n clusters. The identified lowest energy Ni_n cluster structures are in good agreement with those reported previously. We then investigated the sequential H_2 dissociative chemisorption on the lowest energy Ni_n clusters. It was found that the energetically preferred dissociation route for H_2 is to interact with the clusters through the on-top sites with a side-on fashion. The dissociation requires virtually no activation energy and the H atoms fall into two neighboring edge sites adjacent to the Ni atom that acts as the active catalytic center. The process is thermochemically favorable. The adsorption site preference follows the sequence of the edge sites, then the hollow sites and finally the on-top sites. We then studied the mobility of the H atoms on the cluster by moving a H atom from one edge to another edge and found the diffusion barrier is relatively small, suggesting that the H atoms on Ni_n clusters are mobile, which is consistent with experimental observations. Upon the sequential H_2 dissociative chemisorption on the Ni_n clusters, the edges sites are first populated and, as the H loading increases, some of the hollow sites and on-top sites are also occupied. The site preferences for H atoms on the Ni_n, Pd_n and Pt_n clusters were found to be distinctively different.

To gain insight into the catalytic activity of Ni_n, Pd_n and Pt_n clusters, we compared the calculated average H_2 dissociative chemisorption energies at full H-saturation. It was found that the dissociative chemisorption energies for all three metal clusters vary in a small range and are essentially independent of the cluster size. The calculated H desorption energies at full H coverage exhibit similar behavior, although the desorption energy for Ni_{13} appears to be higher than for Pd_{13} and Pt_{13}. Our calculations indicate that the H capacity of small Ni_n clusters is similar to that of small Pd_n clusters but significantly smaller than the H capacity of Pt_n clusters.

Acknowledgments The work conducted at China University of Geosciences was supported by the National Natural Science Foundation of China. (Grant No. 20973159). R. C. F. acknowledges support by the National Science Foundation (Grant No. PHY-0854838). The work at NUS (National University of Singapore) was supported by a NUS start-up fund.

References

1. Doyle AM, Shaikhutdinov SK, Jackson SD et al (2003) Angew Chem Int Ed 42:5240–5243
2. Cuevas F, Joubert JM, Latroche M et al (2001) Appl Phys A Mater Sci Process 72:225–238
3. Chartouni D, Kuriyama N, Kiyobayashi T et al (2002) Int J Hydrogen Energy 27:945–952
4. Lin YM, Rei MH (2000) Int J Hydrogen Energy 25:211–219
5. Chen SC, Hung CCY, Tu GC et al (2008) Int J Hydrogen Energy 33:1880–1889
6. Chen LA, Zhou CG, Wu JP et al (2009) Front Phys China 4:356–366
7. Bertani V, Cavallotti C, Masi M et al (2000) J Phys Chem A 104:11390–11397
8. Roques J, Lacaze-Dufaure C, Mijoule C (2007) J Chem Theory Comput 3:878–884
9. D'Anna V, Duca D, Ferrante F et al (2009) Phys Chem Chem Phys 11:4077–4083
10. Liu X, Dilger H, Eichel RA et al (2006) J Phys Chem B 110:2013–2023
11. Cheng HS, Chen L, Cooper AC et al (2008) Energy Environ Sci 1:338–354
12. Chen L, Cooper AC, Pez GP et al (2007) J Phys Chem C 111:5514–5519
13. Zhou CG, Wu JP, Nie AH et al (2007) J Phys Chem C 111:12773–12778
14. Zhou CG, Yao SJ, Wu JP et al (2009) J Comput Theor Nanosci 6:1320–1327
15. Zhou CG, Yao SJ, Wu JP et al (2008) Phys Chem Chem Phys 10:5445–5451
16. Apsel SE, Emmert JW, Deng J et al (1996) Phys Rev Lett 76:1441–1444
17. Khanna SN, Beltran M, Jena P (2001) Phys Rev B 64:235419
18. Liu SR, Zhai HJ, Wang LS (2002) Phys Rev B 65:113401
19. Gerion D, Hirt A, Billas IML et al (2000) Phys Rev B 62:7491–7501
20. Mark BK (2002) J Chem Phys 116:9703–9711
21. Alonso JA (2000) Chem Rev 100:637–677
22. Estiu GL, Zerner MC (1996) J Phys Chem 100:16874–16880
23. Parks EK, Zhu L, Ho J et al (1994) J Chem Phys 100:7206–7222
24. Reuse FA, Khanna SN (1995) Chem Phys Lett 234:77–81
25. Desmarais N, Jamorski C, Reuse FA et al (1998) Chem Phys Lett 294:480–486
26. Michelini MC, Diez RP, Jubert AH (2001) Int J Quantum Chem 85:22–33
27. Michelini MC, Diez RP, Jubert AH (2004) Comput Mater Sci 31:292–298
28. Baletto F, Ferrando R (2005) Rev Mod Phys 77:371–423
29. Futschek T, Hafner J, Marsman M (2006) J Phys Condens Matter 18:9703–9748
30. Ashman C, Khanna SN, Pederson MR (2003) Chem Phys Lett 368:257–261
31. Swart I, de Groot FMF, Weckhuysen BM et al (2008) J Phys Chem A 112:1139–1149
32. Perdew JP, Wang Y (1992) Phys Rev B 45:13244–13249

33. Perdew JP, Burke K, Ernzerhof M (1996) Phys Rev Lett 77:3865–3868
34. Delley B (1996) J Phys Chem 100:6107–6110
35. Delley B (2000) J Chem Phys 113:7756–7764
36. Dolg M, Wedig U, Stoll H et al (1987) J Chem Phys 86:866–872
37. Bergner A, Dolg M, Kuchle W et al (1993) Mol Phys 80:1431–1441
38. Delley B (1990) J Chem Phys 92:508–517
39. Hirshfeld FL (1977) Theor Chim Acta 44:129–138
40. Halgren TA, Lipscomb WN (1977) Chem Phys Lett 49:225–232
41. Nosé S (1984) Mol Phys 52:255–268
42. Michelini MC, Diez RP, Jubert AH (1998) Int J Quantum Chem 70:693–701
43. Michelini MC, Diez RP, Jubert AH (1999) J Mol Struct 490:181–188
44. Nie AH, Wu JP, Zhou CG et al (2007) Int J Quantum Chem 107:219–224
45. Luo C, Zhou CG, Wu JP et al (2007) Int J Quantum Chem 107:1632–1641
46. Kittel C (2005) Introduction to Solid State Physics, 8th edn. Wiley, New York